Journal of Colloid and Interface Science **234,** 284–292 (2001)
doi:10.1006/jcis.2000.7276, available online at http://www.idealibrary.com on IDEAL®

Simulation of the Adhesion of Particles to Surfaces

Kevin Cooper,*[,1] Anand Gupta,† and Stephen Beaudoin*[,2]

**Department of Chemical and Materials Engineering, Arizona State University, Tempe, Arizona 85287; and †SpeedFam-IPEC Corporation, Chandler, Arizona 85226*

Received November 1, 1999; revised October 16, 2000

The removal of micrometer and submicrometer particles from dielectric and metal films represents a challenge in postchemical mechanical polishing cleaning. Proper modeling of the adhesive force between contaminant particles and these films is needed to develop optimal solutions to postchemical mechanical polishing cleaning. We have previously developed and experimentally validated a model to describe the adhesion between spherical particles and thin films. This simulation expands previous models to characterize the adhesive interaction between asymmetrical particles, characteristic of a polishing slurry, and various films. Our simulation accounts for the contact area between particles and substrates, as well as the morphology of the surfaces. Previous models fail to accurately describe the contact of asymmetrical particles interacting with surfaces. By properly accounting for nonideal and geometry and morphology, the simulation predicts a more accurate adhesive force than predictions based upon an ideal van der Waals model. The simulation is compared to experimental data taken for both semi-ideal particle–substrate systems (polystyrene latex spheres in contact with silicon films) and asymmetrical systems (alumina particles in contact with various films). © 2001 Academic Press

Key Words: **particle adhesion; van deer waals forces; postchemicals mechanical polishing cleaning; semiconductor processing; chemical mechanical polishing.**

INTRODUCTION

In the semiconductor industry, micrometer and submicrometer particle surface contamination can cause device failure and lower process yield. As circuit linewidths continue to decrease, removal of these particles becomes increasingly important. In order to develop optimal methods to remove particles, models to quantify the adhesive forces that hold particles to surfaces are needed.

Adhesive forces have been classified by Krupp (1). *Class I* includes intermolecular forces such as van der Waals (vdW) interactions. *Class II* includes various chemical bonds, including hydrogen bonds. *Class III* includes sintering effects such as diffusion and condensation and diffusive mixing. When studying polymer systems, interdiffusion and entanglement of polymer chains across the interface are considered Class III interactions.

Class I forces, in particular vdW forces, are present in all systems and are generally considered the controlling force in particle adhesion. Therefore, theories to describe particle adhesion focus on quantifying vdW interactions. The current accepted method to predict particle adhesion is to determine the system's Dupré work of adhesion and insert this value into the proper equilibrium model, such as the Johnson–Kendall–Roberts (JKR) (2), Maugis–Pollock (MP) (3), or Derjaguin–Mueller–Toporov (DMT) (4) models. This approach characterizes ideal systems in inert environments with a high degree of certainty. Ideal systems are systems where the geometries of the interacting surfaces are well characterized, the interacting area is smooth with uniform chemical properties, and the only force present is the vdW dispersion force. However, when the system deviates from ideal conditions, model predictions disagree with experimental data. Therefore, a more comprehensive method to describe particle adhesion is needed. Below is a description of the current accepted method to predict particle adhesion, a review of the limitations of this approach, and a detailed description of our simulation. Our simulation advances the current approaches to better account for geometry, surface morphological and chemical heterogeneities, and surface mechanical properties. It also provides statistical information about observed variations in the adhesion force. Current approaches predict a singular value for the adhesive force for a given system and do not account for observed variances in removal forces.

The surface force apparatus (SFA), the atomic force microscope (AFM), and the interfacial force microscope (IFM) have provided direct methods to measure the force to separate contacting surfaces. They have allowed the measurement of particle adhesion for both ideal and nonideal systems. Measured removal forces for ideal systems agree with predictions made using one of the equilibrium models described above (5–7). However, most systems of interest are not ideal. Instead, these systems generally exhibit surface roughness and asymmetrical geometries and are influenced by other forces in addition to dispersion forces. Measured removal forces for nonideal systems vary between one and three orders of magnitude from predictions made using one of the equilibrium models.

When experimental measurements differ drastically from predictions based upon one of the equilibrium models, the

[1] Current address: Advanced Product Research and Development Laboratory, Semiconductor Products Sector, Motorola, 3501 Ed Bluestein Blvd. MD K-10, Austin, TX 78721.

[2] To whom correspondence should be addressed.

0021-9797/01 $35.00
Copyright © 2001 by Academic Press
All rights of reproduction in any form reserved.

reason most commonly given is nonideal surface morphology (8, 9). Recently, there have been a number of investigations into the effect of surface morphology on colloidal forces inside and outside of contact. Walz has published a literature review that describes the work in the area (10). Several groups have focused on modeling the effect of surface morphology on colloidal forces outside of contact (11–16) but there have been only a few investigations modeling the effect of surface morphology on adhesion.

Fuller and Tabor (17) modeled the adhesion of a smooth flat surface in contact with a rough flat surface. They modeled roughness as asperities with equal radius of curvature but with a Gaussian distribution in heights and employed the JKR equilibrium theory to calculate the removal force for each individual asperity. They also quantified the effect of dispersity in asperity heights on adhesion. By adjusting a parameter that represented the dispersity in asperity heights, they were able to fit data they collected for the adhesion between optically smooth rubber spheres and hard, flat, surfaces of Perspex with various degrees of roughness. They found that removal force decreased as the polydispersity in asperity heights increased. This agrees with data obtained in our lab, where the adhesion between rough polystyrene latex (PSL) spheres and rough and smooth silicon surfaces was measured with an AFM (18). As the roughness of the silicon surface increased, the removal force decreased, and we attributed this result to a reduced mass interacting in the interfacial area. Mizes (19) and Sasaki (8) obtained similar results by measuring both the localized topography and the localized adhesive forces between various planar surfaces and an AFM cantilever with a pyramid-shaped tip (radius of curvature $<0.03\ \mu$m). Mizes found that on high points on the planar surfaces where the AFM tip had very little mass interacting with the surfaces, adhesion forces were lowest. On pits or depressions where the cantilever had more mass interacting with the surfaces, he found that adhesion forces were highest. He modeled this fluctuation in adhesive force by correcting the equilibrium model predictions to account for changes in the curvature of the planar surfaces, given by

$$\frac{\delta F}{F} = R_t \delta C_s, \qquad [1]$$

where δF is the fluctuation in the local adhesion force, R_t is the radius of curvature of the AFM cantilever, and δC_s is the fluctuation in the surface curvature. Sasaki detailed the relation between tip position and the adhesion by conventional JKR models.

Schaefer *et al.* measured the removal force between glass, PSL, and tin spheres and atomically smooth mica and highly oriented pyrolitic graphite surfaces with an AFM (20). The values they measured were $\sim$50 times less then expected based on JKR theory and they attributed the difference to surface morphology of the particles. They proceeded to quantify the surface morphology of the individual particles using AFM line scans. This allowed them to calculate the radius of curvature of individual asperities, which they plugged into the JKR theory to predict a removal force for each asperity. By summing the removal force of all the asperities, they obtained a removal force that still overpredicted the measured removal force by a factor of three.

The approaches described above are a good foundation for developing comprehensive descriptions of the effect of surface morphology on particle adhesion. However, these studies do not provide an accurate description of the adhesive force for nonideal particles. First, much of this work was developed for the interaction between either smooth surfaces or one rough surface and one smooth surface. In real systems both surfaces have a certain degree of roughness. Second, the above work models asperities as spherical particles distributed over the surfaces. Roughness on real surfaces can have set geometric patterns, random roughness patterns, or complex fractal patterns (21). Third, this work does not account for compression and deformation of surface asperities resulting from either the adhesive force or the adhesive force summed with an external applied load. By estimating the compression of asperities on the surface of PSL particles interacting with silicon surfaces using the JKR model, Schaefer (20) concluded that compression would not significantly alter the asperities' shape and therefore would not influence the removal forces. Following a similar approach, Biggs (22) determined that under certain conditions the load would cause substantial compression of the asperities.

The existing models describe only the interaction of spherical, elastic particles with substrates. Real particles are asymmetrical and can consist of rigid, elastic, elastoplastic, or plastic materials. Figure 1 is a scanning electron micrograph (SEM) of an alumina particle on a silicon surface. Currently, alumina slurry particles represent a contamination problem during chemical mechanical polishing (CMP) in semiconductor processing. These particles are rigid and asymmetrical, and they adhere strongly to silicon surfaces. Current adhesion models could not account for the geometry, morphology, or mechanical properties of these particles. The work presented here, which couples computer simulation with a fundamental adhesion model, was designed to predict the adhesive interactions for ideal and real particles by accounting for particle and surface morphology, compression, and asymmetry, as well as variations in deformation behavior.

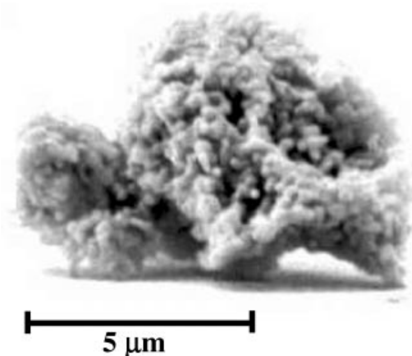

FIG. 1. Scanning electron micrograph of an alumina particle.

Model Description

Our model predicts the adhesive interactions between two surfaces of arbitrary shape, each with localized chemical and morphological heterogeneities. The basic procedure for our simulation involves constructing a mathematical description of two solid surfaces, bringing the surfaces toward each other so that vdW interactions may be important and then summing the vdW interactions calculated between individual volume elements in the two surfaces. The calculations are performed on a desktop computer using a C++ code developed at ASU. Figure 2 is a schematic outlining the procedure. The specific steps are described in more detail here.

1. Macroscopic Surface Description

The first step in our simulation is to assume both surfaces are atomically smooth and determine the area in contact between the interacting solids based only on their geometry. These contact regions, when modified to account for morphological effects, control the magnitude of the adhesion force. As a particle is withdrawn from a surface, two factors determine the contact area immediately prior to particle removal. These factors are the type of deformation the particle undergoes and the separation mechanism when the particle is pulled from the surface. Separation can either occur at the interface ("brittle" or adhesive rupture) or within the softer of the two materials ("ductile" or cohesive rupture) (3). Contact area at pull-off is not well understood during brittle rupture. AFM studies by Biggs and Spinks suggest that brittle rupture occurs at slow pull-off speeds and large applied loads (28). We have designed our model and experiments to simulate ductile rupture based on molecular dynamic simulations of instantaneous adhesive rupture interactions involving PSL spheres and various substrates (23). According to Maugis and Pollock, separation for ductile rupture occurs at the maximum contact area achieved between the colloid and the substrate (3).

Our simulation determines the contact area by one of two different approaches depending upon the characteristics of the particle being studied. Case I is for the interaction of flat surfaces with spherical particles that have been allowed to settle on the surface for an extended period of time and for which the deformation of the particle or substrate has been modeled. This case considers ideal geometries. Case II is for asymmetrical particles. This case determines the contact area of the particle by CAD volume reconstruction of the particle from SEM micrographs. In all cases the separation is assumed to be ductile.

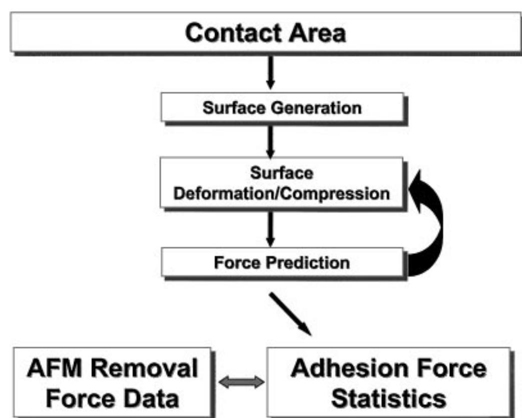

FIG. 2. A schematic diagramming the procedure for the adhesion simulation.

Case I: Ideal geometries, contact area based on observation. Rimai *et al.* (24) designed experiments that used an SEM to measure the contact radius, ca, of spherical particles on surfaces for particles of varying radii. From their data, they were able to model the contact radius as a function of particle radius. In prior work, we used this approach to model the contact area as a function of particle radius for PSL spheres in contact with a silicon (with surface oxide) surface (25). The result is:

$$\mathrm{ca}(\mu\mathrm{m}) = 0.24 * R(\mu\mathrm{m})^{0.5}. \quad [2]$$

This model can be used in our simulation to determine the contact area between PSL spheres and silicon surfaces that have been in contact for long times.

For spherical particles that deform, this is a convenient way to determine contact area. This is because this method does not require knowledge of material properties or initial values for simulation iterations.

Case II: Nonideal geometries. This case provides an estimate of contact area for particle–substrate interactions when particles with asymmetrical geometries, such as shown in Fig. 1, are present. It estimates the geometry of the contact region based on AFM and SEM images of the particle. Specifically, we construct a mathematical representation of the surface of the particle from the images, rotate the mathematical particle representation to simulate how it settles on the surface, and then predict the contact area between the particle and the substrate. Figure 3 displays an alumina particle that is mounted onto an AFM cantilever. The left side of Fig. 3 is a reconstructed 3D image of the surface of the alumina particle. The right image in Fig. 3 is a field emission (FESEM) of that particle.

The reconstruction shown in the left side of Fig. 3 was accomplished with an imaging software package (PhotoModeler). By reconstructing the surface in this manner we are able to obtain a mathematical representation of the surface (26). After the particle was reconstructed, it was rotated around its lowest point until three separate points on the particle could contact the substrate. This is only an approximation of how a particle settles, but it is adequate for this first simulation. Once we finished rotating the particle, the contact area was estimated by determining the area of the peaks that touched the surface. This value was then inserted into our simulation.

2. Microscopic Surface Generation

Once the geometric contact area between the particle and substrate was determined, the second step was to simulate (based

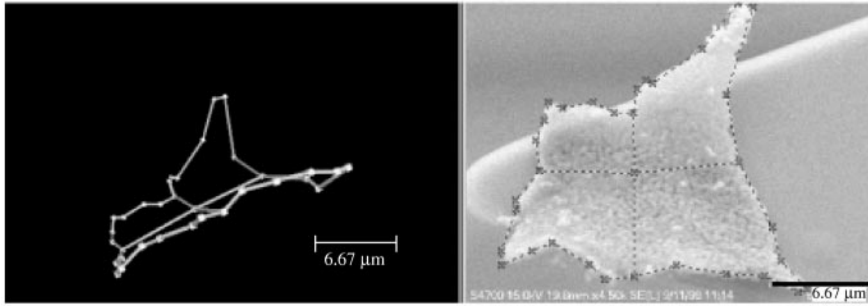

FIG. 3. An alumina particle mounted onto an AFM cantilever. The right image is an uncoated FE image of the AFM cantilever with alumina particle. The left image is a 3D reconstruction of the same particle.

on experimentally measured parameters) the surface morphology of the two interacting surfaces.

The morphology of the two interacting surfaces was characterized by an AFM used in topographic mode. Four parameters of each surface were determined from the AFM scans: the presence of a common asperity shape on each surface (if any), the average size of the asperities, the variance in the asperity size, and the fractional coverage of the surface by asperities. When there was no common asperity shape, as was the case in this study, the asperities were assumed to be hemispherical. The size, variance in size, and fractional coverage of the surface were calculated by scanning a set area of a surface and then evaluating all asperity peaks in that area. The scan area for our measurements was 100 nm^2. This area was small enough that the curvature of the particles was not a factor in the measurements.

In the simulation, rough surfaces were generated by a method similar to one developed by Bhattacharjee (11). First, a flat surface (with an area equal to the contact area estimated in step 1) was generated. Next a hemispherical asperity was placed at a random location on the surface. The size of the asperity was randomly selected from a normal distribution of asperity heights. The normal distribution was centered at the mean observed asperity size, μ, and had a standard deviation, σ, corresponding to our experimental measurements. After each asperity was placed on the surface, the fractional coverage of the surface was calculated. If the coverage was not equal to the measured fractional coverage, fc, the procedure was repeated. Figure 4 is a topographical map of a rough surface generated in this fashion with $\mu = 15$ nm, $\sigma = 5$ nm, and fp = 80%. This procedure was used to place random asperities on the surface to simulate actual surfaces.

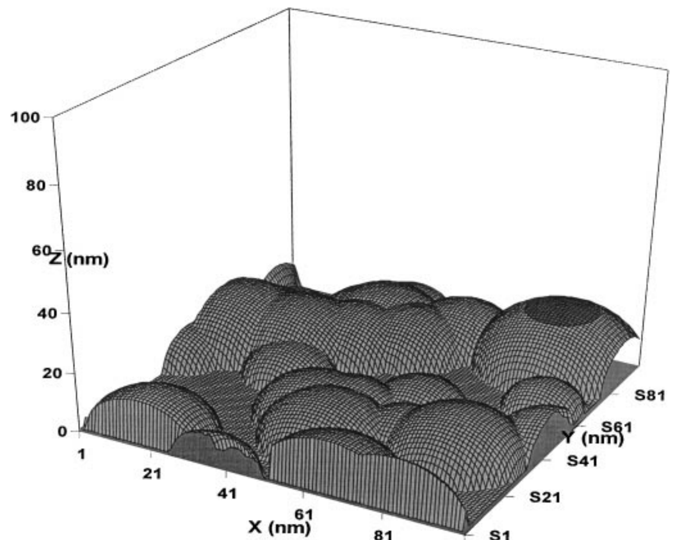

FIG. 4. An illustration of the topography of a 100 nm by 100 nm surface covered with asperities (fc 80%, $\mu = 15$ nm, $\sigma = 5$ nm).

3. *Allowing the Surfaces to Interact*

Once mathematical representations of both surfaces were generated, the surfaces were brought into close proximity and an adhesive force was calculated. This procedure consisted of the following steps:

1. Bring the two surfaces together until a single contact point, cp, is reached. Figure 5 is a schematic depicting the interaction of two rough surfaces at this condition.

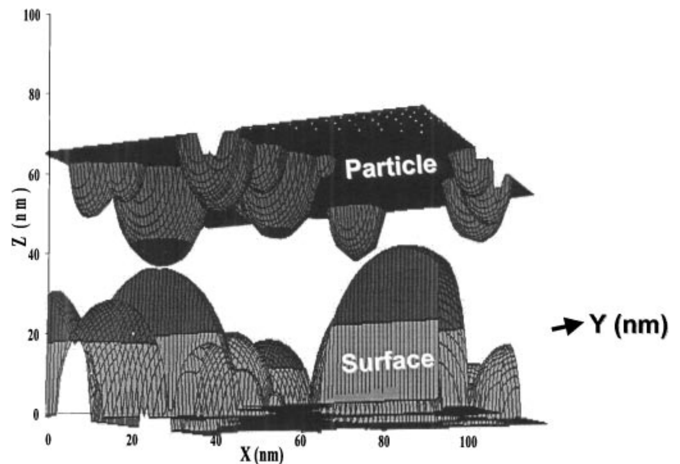

FIG. 5. A schematic of the interaction between a rough particle and a rough surface.

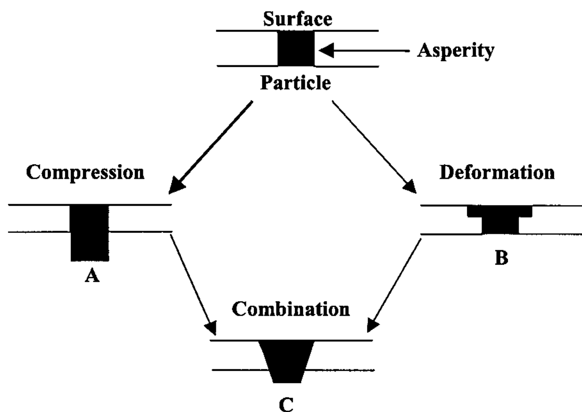

FIG. 6. A schematic of three types of asperity compression.

2. Compress the asperities on the softer of the surfaces if any external load is present. Any vdW effects are not considered until later.
3. Calculate the adhesive force between the surfaces based on vdW interactions.
4. Return to step 2 and recompress the surface asperities to compensate for the adhesive force.
5. Recalculate the force.

Steps 2–5 were repeated until the change in the calculated adhesive force was less then one percent.

As mentioned by Biggs (22), compression of asperities is a complex problem that involves both bulk material collapse and asperity deformation. To account for asperity compression we focused on two opposite extremes of asperity behavior. Figure 6 is a schematic of the types of compression considered. The first type of asperity compression represents the surfaces coming closer together as a result of an increase in the density of the softer material (Fig. 6A). The second type of compression represents the flattening of the surface of the softer of the two materials by the load (Fig. 6B). The actual compression is expected to be a combination of these extreme cases (Fig. 6C). Our simulation estimates the compression by averaging predictions based on the two extremes.

The interaction force was calculated from a macroscopic, or pairwise additive, approach. This approach divided the particle into individual volume elements, each a different distance D from the surface. The vdW force for each element was then calculated. The total adhesive force was the sum of the forces from the individual volume elements. Cylindrical elements were used, as depicted in Fig. 7.

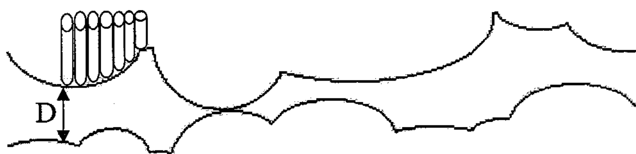

FIG. 7. A schematic of the cylindrical volume elements in our simulation.

The force between a cylindrical volume element and a substrate was calculated from

$$F_{\mathrm{attr}} = -\frac{A \cdot (\text{Area cylinder})}{6 \cdot \pi \cdot D^3}, \qquad [3]$$

where F_{attr} is the adhesive force (N) and A is the system's Hamaker constant. Cylindrical volume elements of 1 nm diameter were used.

The models just described use a vdW formulation to account for the interfacial interactions between a particle and a substrate. The key parameters in the calculation are the Hamaker constant of the system and the compressibility, geometry, morphology, and deformation behavior of the interacting surfaces.

To validate our simulation, we conducted two separate sets of experiments. In the first set of experiments we measured the interaction force between PSL spheres and silicon substrates in aqueous solution (18, 25). These experiments can be described by the contact area model in Case I. In the second set of experiments we measured the interaction force between an asymmetrical alumina particle and both a SiO_2 and a Cu substrate. These experiments can be described by the contact area model in Case II.

EXPERIMENTAL PROCEDURE

The results presented here and the complete experimental procedure employed to obtain these results have been previously published (18, 25). Below is a review of the experimental procedure.

An AFM was used to measure the removal force for these systems. The PSL and alumina particles were mounted on an AFM cantilever by a modified version of the technique developed by Ducker (27, 28). The spring constants of the cantilevers were determined by a method developed by Cleveland *et al.* (29). Once the particles were mounted on the cantilevers and the spring constants of the cantilevers were determined, each cantilever with mounted particle was inserted into the AFM. Next the AFM was employed to bring the particles into contact with the substrate and to measure the removal force. During these measurements both the applied load and the contact time were carefully controlled. SEM micrographs of the particles were obtained to determine the size, the contact area, and the mass of the particles. The AFM was employed in topographic mode to measure the roughness of the colloids and surfaces.

RESULTS AND DISCUSSION

Case I of our simulation is compared against two different sets of experimental data. The first set of data documents the adhesion interaction between PSL spheres and silicon substrates in deionized water. This system represents the interaction of one rough, deformable surface (PSL) with a second smooth rigid surface (silicon). The second set of data documents the adhesion interaction between PSL spheres and silicon substrates in

an aqueous KNO_3 solution at pH values from 2 to 10. The solutions were prepared by combining HNO_3 and KOH at a constant ionic strength of 0.03 M. Since the KNO_3 etches the silicon at elevated pH values, this system represents the interaction of two rough surfaces. In both cases, the silicon was covered with a surface oxide film, as described elsewhere (18). Case II is compared against experimental data for the interaction between an Al_2O_3 particle and polished SiO_2 and Cu substrates in dry N_2 and aqueous environments.

Case I assumed that the PSL spheres deformed to their equilibrium level on the surface before they were removed. This allowed the contact area established between the spheres and surface to be predetermined based on the model of SEM contact area data, as previously described (25) and shown in Eq. [2]. By studying the shape of AFM force curves when particles are withdrawn from surfaces, Biggs and Spinks were able to predict what type of deformation particles underwent (22). However, the amount a particle deforms when in contact with a surface in different media has not been comprehensively modeled as a function of applied load and contact time. Therefore, although our assumption that the particle completely deforms under minimal contact time and applied load may not be entirely accurate, it represents one limiting case of behavior.

The following parameters were used in the simulation: $A = 3.2 * 10^{-20}$ J (25), Lennard-Jones separation = 0.4 nm (30), E (PSL) = $3 * 10^9$ N/m^2 (24), and applied load = 50 nN. The topography of the PSL also was included (fractional coverage, fc = 30%; mean asperity size, $\varepsilon = 5.56$ nm; standard deviation in asperity size, std = 4.38 nm).

Figure 8 displays a histogram of 10,000 model predictions for the adhesive force for a 5-μm radius PSL sphere interacting with a smooth silicon substrate in DI water. Each of these predictions is for a $R = 5$-μm particle, but with a random distribution of asperities constrained by the experimentally determined parameters fc = 30%, $\varepsilon = 5.56$ nm, and std = 4.38. Figure 8 shows a peak around 124 nN which tails off quickly. The simulation predicts an average removal force of 120 nN, with a standard deviation of 24.4 nN. Our measured removal force for this system was 127 ± 20.7 nN (25). This represents excellent agreement in both average value and variance. Other studies reviewed exhibit similar distributions in removal force measurements (31, 32).

Figure 9 is a comparison of the measured and predicted removal forces for PSL spheres in contact with silicon in DI water as a function of particle radius (25). Each data point is the average of 50 removal force measurements. The solid black line in Fig. 9 is the average value predicted by our simulation employing Eq. [3]. The upper and lower dashed lines in Fig. 9 are one standard deviation from the average prediction. Three important points can be drawn from Fig. 9. First, Fig. 9 shows our simulation's ability to predict the removal force for the interaction of a rough particle with a smooth surface. Second, it displays our simulation's ability to predict the variance in the measured removal force. Third, the agreement between experiment and prediction is accomplished with only measured parameters, and no adjustable parameters, in our equations.

In our previous work, we measured the removal force between 5 μm radius PSL spheres and a silicon surface (with surface oxide) as a function of pH in a 0.03 M KNO_3 solution (18). At low pH values the surface remained atomically smooth and the adhesive force was similar to the values shown above in Fig. 9 (127 ± 20.7 nN). However, at pH values greater than 5, the silicon surface was etched by the KOH leaving behind a

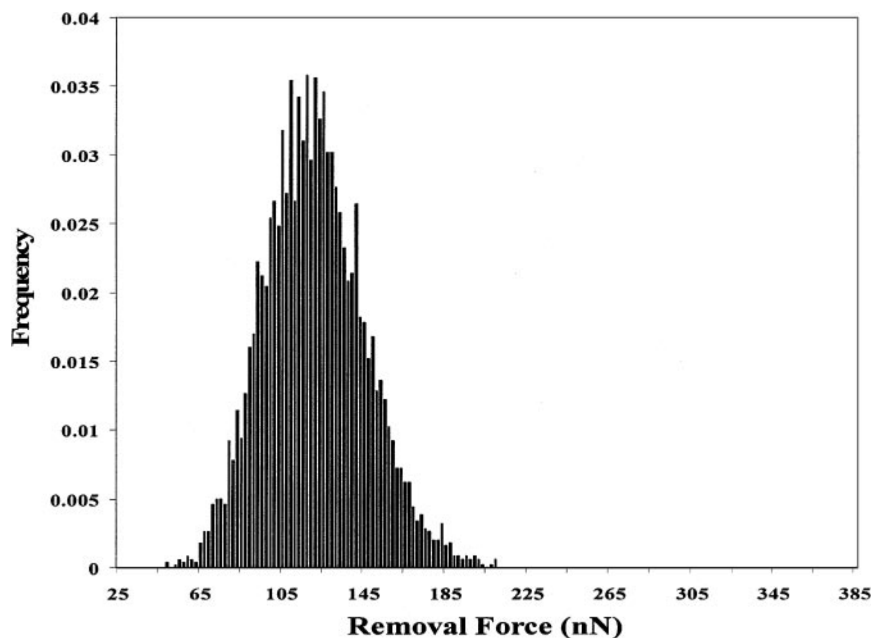

FIG. 8. The frequency of occurrence of removal force (nN) for the interaction of a $R = 5$-μm PSL sphere with a smooth silicon surface in DI water.

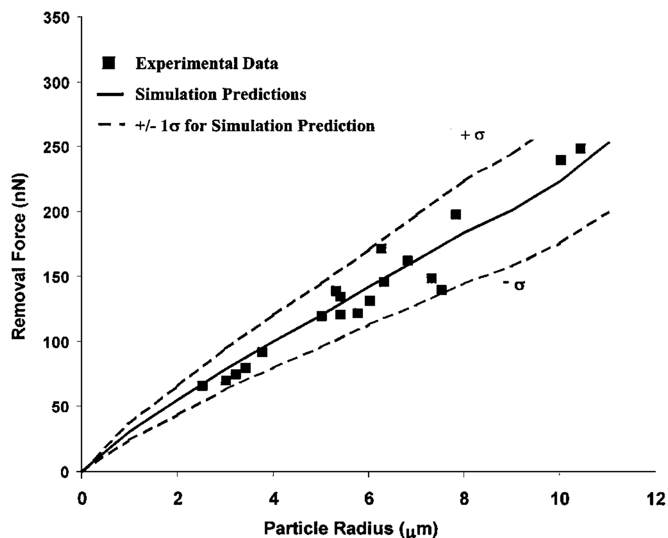

FIG. 9. Predicted and observed removal force as a function particle radius for PSL spheres interacting with smooth silicon surfaces in DI water. The black squares are the average of 50 measured values. The solid black line is the average of 5000 simulated particle surface interactions. The upper and lower dashed lines are one standard deviation from the predictions.

rough surface. The adhesion force at these pH values was barely measurable (∼10 nN). The topography of the silicon surface at pH values greater than 5 was measured as having a fractional asperity coverage, fc, of 20%, a mean asperity size, ε, of 25 nm, and a standard deviation in asperity size, std, of 20 nm. The outermost surface of the silicon was an oxide throughout the pH

TABLE 1
Surface Roughness of Materials in Our Study

Material	ε_s (nm)	Std (nm)	Frac. coverage
SiO_2	1.7	0.7	0.01
Cu	53.8	25.2	0.33
Al_2O_3 particle	1.6	0.7	0.03

range (18). Figure 10 compares the observed adhesive force to predictions, based on our simulation, for both the case where the silicon surface is atomically smooth ($F = 127$ nN) and the case where the silicon is rough, with topography characterized by the above measured values ($F \sim 10$ nN). As can be seen, the substrate roughness dramatically influenced the observed and predicted adhesive interaction between the particle and the substrate.

In the second group of experiments, an AFM was employed to measure the removal force between an alumina particle (as shown in Fig. 3) and polished SiO_2 and Cu substrates in dry N_2 and deionized water. The morphologies of the SiO_2 and Cu substrates and the alumina particle were measured with an AFM operated in topographic mode and are provided in Table 1. Figure 11 displays topographic AFM images of the polished SiO_2 and polished Cu substrates. As can be seen, there is a significant difference in the roughness on these two surfaces. The SiO_2 is approximately atomically smooth, while the Cu has a substantial amount of surface roughness.

In addition to the parameters in Table 1, the following parameters were used to simulate the adhesion between alumina

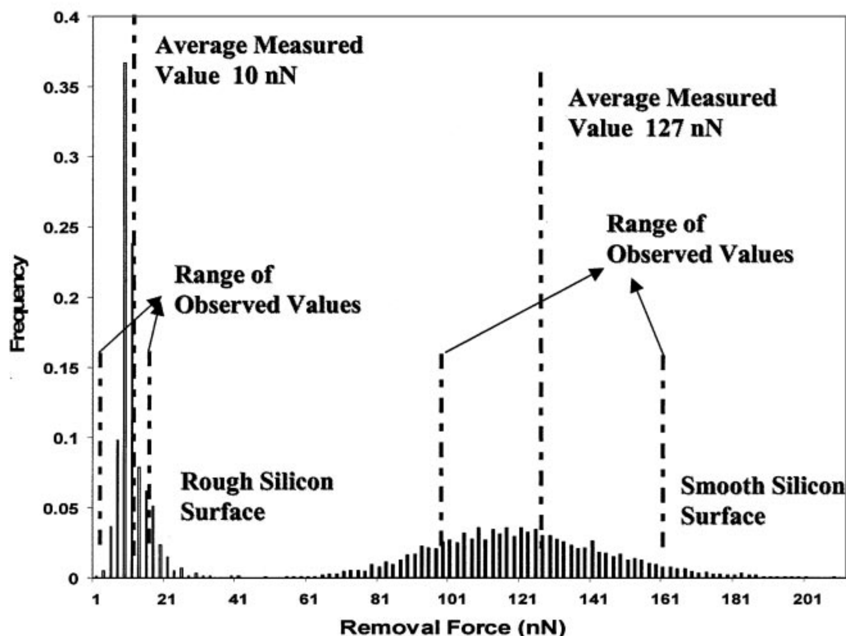

FIG. 10. Predicted and observed frequency of occurrence of removal force (nN). The peaks from 0 to 30 nN are for the interaction between a rough $R =$ 5-μm PSL sphere (fc 30%, $\mu = 5.56$ nm, $\sigma = 4.38$ nm) and a rough silicon surface (fc 20%, $\mu = 25$ nm, $\sigma = 20$ nm). The peaks from 50 to 200 nN are for the interaction between a rough $R = 5$-μm PSL sphere (fc 30%, $\mu = 5.56$ nm, $\sigma = 4.38$ nm) and a smooth silicon surface.

particles and SiO_2 and Cu substrates: {$A = 21.7 * 10^{-20}$ J ($Cu/N_2/Al_2O_3$), $9.7 * 10^{-20}$ J ($SiO_2/N_2/Al_2O_3$), $6.2 * 10^{-20}$ J ($Cu/H_2O/Al_2O_3$), $1.3 * 10^{-20}$ J ($SiO_2/H_2O/Al_2O_3$) [33–37]}, Lennard-Jones separation = 0.4 nm, $E = 5 * 10^{11}$ N/m^2 for the Al_2O_3 and SiO_2 and $1.2 * 10^{11}$ N/m^2 for the Cu [38; 39], and applied load = 1500 nN. The contact areas between the particle and the substrates were estimated using the 3D-reconstruction method outlined above. In both cases, the area of contact was 600 nm. The particle was estimated to have a volume of 25.2 μm^3, which corresponds to a spherical particle of radius $R = 1.8$ μm. Each simulation is the average 1000 model predictions.

Figure 12 compares experimental measurements with predictions from our simulation and from an ideal vdW model ($F = AR/6D^2$). The dashed lines in Fig. 12 are the predictions from the ideal vdW model for a spherical alumina particle of radius 1.8 μm. The solid lines are the average predictions based on our simulation and the box represents 1 standard deviation in our simulation prediction.

Figure 12 shows that our simulation is in better agreement with experimental data than predictions based on an ideal vdW model for the alumina/SiO_2 system. For the alumina/Cu system, although the average prediction for our simulation and an ideal vdW model show reasonable agreement with the average measured force, our simulation accurately describes the observed variance in removal force. Traditional models (vdW and equilibrium models) provide a singular prediction for removal force. Figure 12 also displays the enormous effect surface roughness can have on both the removal force and the variance in the removal force. For smooth systems (SiO_2 substrate), a narrow range of removal forces is both predicted and observed. However, as the roughness increases, the range of observed and predicted removal forces increases (Cu substrate). This results from the fact that the two interacting surfaces have an increased number of potential configurations when in contact.

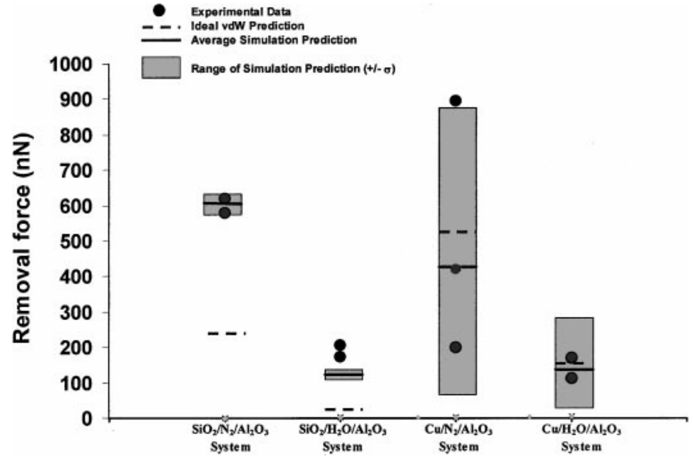

FIG. 12. Predicted and observed removal forces for alumina particles on SiO_2 and Cu substrates in dry N_2 and aqueous environments. The dashed lines are predictions based upon an ideal vdW model. The solid lines are the average prediction from our simulation and the shaded area is the range of our prediction within 1 standard deviation of the average prediction.

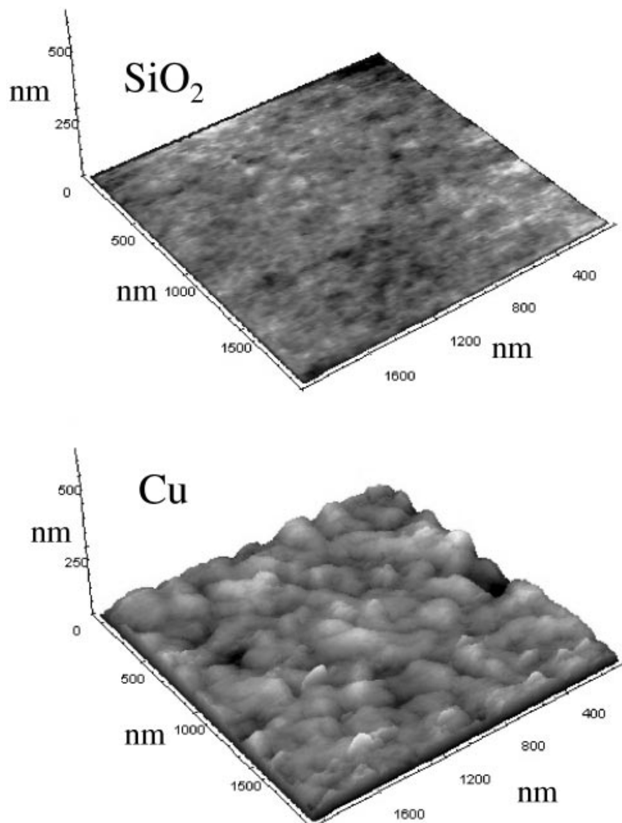

FIG. 11. Topographic AFM scans of SiO_2 and Cu in our study.

CONCLUSION

We have developed and experimentally validated a simulation that predicts particle adhesion in aqueous and dry environments. This simulation is an extension of vdW analysis that better accounts for the effects of particle and substrate surface morphology and mechanical properties. The predictions generated in our work can be incorporated into comprehensive models to describe particle removal processes. The simulation is not limited to describing the adhesive interaction between spherical elastic particles and rigid surfaces but has been shown to predict the interaction for other particle–surface combinations whose physical characteristics can be assessed.

ACKNOWLEDGMENTS

The authors are grateful to Speedfam-IPEC Corporation, to the National Science Foundation (CTS-9984620), and to the National Science Foundation Semiconductor Research Corporation Center for Environmentally-Benign Semiconductor Manufacturing (EEC-9528813) for both financial support and technical guidance on this project. The authors are also grateful to Dr. B. L. Ramakrishna of ASU, Director of the Center for Interactive Nano-Visualization in Science and Engineering Education, for providing both assistance and equipment and facilities (NSF/REC 9632740 and NSF/DUE9551558) on this project, and to the Centers for Solid State Electronics Research and Solid State Science

at ASU. Finally, the authors are grateful to Frank Dunn for his assistance in the computer programming and to Dr. Anand Gupta at SpeedFam-IPEC for his insight in these studies.

REFERENCES

1. Krupp, H., *Adv. Colloid Interface Sci.* **1,** 111 (1967).
2. Johnson, K. L., Kendall, K., and Roberts, A. D., *Proc. Roy. Soc. London A* **324,** 301 (1971).
3. Maugis, D., and Pollock, H. M., *Acta Metall.* **32,** 1323 (1984).
4. Derjaguin, B. V., Muller, V. M., and Toporov, Y. P., *J. Colloid Interface Sci.* **53,** 314 (1975).
5. Israelachvili, J. N., and Tabor, D., *Proc. Roy. Soc. London A* **331,** 19 (1972).
6. Mangipudi, V. S., Huang, E., and Tirrell, M., *Macromol. Symp.* **102,** 131 (1996).
7. Chaudhury, M. K., and Whitesides, G. M., *Langmuir* **7,** 1013 (1991).
8. Sasaki, M., Hane, K., Okuma, S., and Torii, A., *J. Vac. Sci. Technol. B* **13,** 350 (1995).
9. Sounilhac, S., Barthel, E., and Creuzet, F., *J. Appl. Phys.* **85,** 222 (1998).
10. Walz, J. Y., *Adv. Colloid Interface Sci.* **74,** 119 (1998).
11. Bhattacherjee, S., Ko, C. H., and Elimelech, M., *Langmuir* **14,** 3365 (1998).
12. Suresh, L., and Walz, J., *J. Colloid Interface Sci.* **183,** 199 (1996).
13. Suresh, L., Ph.D. thesis Tulane University, 1997.
14. Czarnecji, J., and Dabros, T., *J. Colloid Interface Sci.* **78,** 25 (1980).
15. Sparnaay, M. J., *J. Colloid Interface Sci.* **91,** 307 (1983).
16. Herman, M. C., and Papadopoulos, K. D., *J. Colloid Interface Sci.* **142,** 331 (1991).
17. Fuller, K. N. G., and Tabor, D., *Proc. Roy. Soc. London A* **345,** 327 (1975).
18. Cooper, K., Gupta, A., and Beaudoin, S., In Press *J. Colloid Interface Sci.* **228,** 213 (2000).
19. Mizes, H. A., *J. Adhesion* **51,** 155 (1995).
20. Schaeffer, D. M., Carpenter, M., Gady, B., Reifenberger, R., Demejo, L. P., and Rimai, D. S., *J. Adhesion Sci. Technol.* **9,** 1049 (1995).
21. Emerson, C. W., Lam, N., and Quattrochi, D. A., *Photo. Eng. Remote Sen.* **65,** 51 (1999).
22. Biggs, S., and Spinks, G., *J. Adhesion Sci. Technol.* **12,** 461 (1998).
23. Bhushan, B., Israelachvili, J. N., and Landman, U., *Nature* **374,** 607 (1995).
24. Rimai, D. S., DeMejo, P., Bowen, R., and Morris, J., *in* “Particle on Surfaces” (K. L. Mittal, Ed.), p. 1. Dekker, New York, 1995.
25. Cooper, K., Ohler, N., Gupta, A., and Beaudoin, S., *J. Colloid Interface Sci.* **222,** 63 (2000).
26. Coombs, G. H., Tetley, L., Moss, V. A., and Vickerman, K., *Parasitology* **92,** 13 (1986).
27. Ducker, W. A., and Senden, T. J., *Langmuir* **8,** 1831 (1992).
28. Ducker, W. A., Senden, T. J., and Pashley, R. M., *Nature* **353,** 239 (1991).
29. Cleveland, J. P., Manne, S., Bocek, D., and Hansma, P. K., *Rev. Sci. Instrum.* **64,** 403 (1993).
30. Busnaina, A., Taylor, J., and Schaeffer, D. M., *J. Adhesion Sci. Technol.* **7,** 441 (1993).
31. Noy, A., Frisbie, D., Rozsnyai, F., Wrighton, M., and Lieber, C., *J. Am. Chem. Soc.* **117,** 7943 (1995).
32. Williams, J., Han, T., and Beebe, T., *Langmuir* **12,** 1291 (1996).
33. Brumfield, J. C., Goss, C. A., and Irene, E. A., *Langmuir* **8,** 2810 (1992).
34. Goss, C. A., Brumfield, J. C., and Irene, E. A., *Langmuir* **8,** 1459 (1992).
35. Ackler, H. D., French, R., and Chiang, Y. M., *J. Colloid Interface Sci.* **179,** 460 (1996).
36. Evans, D. F., and Wennerstrom, H., “The Colloidal Domain.” VCH, New York, 1994.
37. Bowling, R. A., *J. Electrochem. Soc.* **21,** 2208 (1985).
38. Chechenin, N. G., Bottiger, J., and Krog, J. P., *Thin Solid Films.* **304,** 70 (1997).
39. Courtney, T. H., “Mechanical Behavior of Materials.” McGraw-Hill, New York, 1990.